Domain Flexibility in Ligand-Free and Inhibitor-Bound *Escherichia coli* Adenylate Kinase Based on a Mode-Coupling Analysis of ^{15}N Spin Relaxation†

Yury E. Shapiro,‡ Edith Kahana,‡ Vitali Tugarinov,‡,|| Zhichun Liang,§ Jack H. Freed,*,§ and Eva Meirovitch*,‡

Faculty of Life Sciences, Bar-Ilan University, Ramat-Gan 52900, Israel, and Baker Laboratory of Chemistry and Chemical Biology, Cornell University, Ithaca, New York 14853-1301

Received December 7, 2001; Revised Manuscript Received March 5, 2002

ABSTRACT: Adenylate kinase from *Escherichia coli* (AKeco), consisting of a 23.6-kDa polypeptide chain folded into domains CORE, AMPbd, and LID catalyzes the reaction AMP + ATP ↔ 2ADP. The domains AMPbd and LID execute large-amplitude movements during catalysis. Backbone dynamics of ligand-free and AP_5A-inhibitor-bound AKeco is studied with slowly relaxing local structure (SRLS) ^{15}N relaxation, an approach particularly suited when the global (τ_m) and the local (τ) motions are likely to be coupled. For AKeco $\tau_m = 15.1$ ns, whereas for AKeco*AP_5A $\tau_m = 11.6$ ns. The CORE domain of AKeco features an average squared order parameter, $<S^2>$, of 0.84 and correlation times $\tau_f = 5-130$ ps. Most of the AKeco*AP_5A backbone features $<S^2> = 0.90$ and $\tau_f = 33-193$ ps. These data are indicative of relative rigidity. Domains AMPbd and LID of AKeco, and loops β_1/α_1, α_2/α_3, α_4/β_3, α_5/β_4, and β_8/α_7 of AKeco*AP_5A, feature a novel type of protein flexibility consisting of nanosecond peptide plane reorientation about the $C^{\alpha}_{i-1}-C^{\alpha}_i$ axis, with correlation time $\tau_\perp = 5.6-11.3$ ns. The other microdynamic parameters underlying this dynamic model include $S^2 = 0.13-0.5$, $\tau_{||}$ on the ps time scale, and a diffusion tilt β_{MD} ranging from 12 to 21°. For the ligand-free enzyme the $\tau_\perp$ mode was shown to represent segmental domain motion, accompanied by conformational exchange contributions $R_{ex} \leq 4.4$ s^{-1}. Loop α_4/β_3 and α_5/β_4 dynamics in AKeco*AP_5A is related to the "energetic counter-balancing of substrate binding" effect apparently driving kinase catalysis. The other flexible AKeco*AP_5A loops may relate to domain motion toward product release.

The ability to interpret nuclear spin relaxation properties in terms of microdynamic parameters turned NMR into a powerful method for elucidating protein dynamics (*1*, *2*). The amide ^{15}N spin in proteins is a particularly useful probe, relaxed predominantly by dipolar coupling to the amide proton and ^{15}N chemical shift anisotropy (CSA)[1] (*3*). The experimental NMR observables are controlled by the global and local dynamic processes experienced by protein N−H bond vectors, which determine the spectral density function, $J(\omega)$. ^{15}N relaxation data in proteins are commonly analyzed with the model-free (MF) approach, where the global and local motions are assumed to be decoupled (*4*−*6*). In a recent study (*7*), we applied the two-body slowly relaxing local structure (SRLS) approach developed by Freed and co-workers (*8*, *9*) to ^{15}N relaxation in proteins. SRLS accounts rigorously for dynamical coupling between the local and global motions, and treats the global diffusion, the local diffusion, the local ordering, and the magnetic interactions as tensors that may be tilted relative to one another, providing thereby important information related to protein structure (*10*−*12*). The MF spectral density functions constitute asymptotic solutions of the SRLS spectral densities (*7*, *8*, *13*). It was found that currently available experimental ^{15}N relaxation data are sensitive to the coupling-induced mixed modes inherent in the SRLS model (*7*, *14*).

AKeco is a particularly intriguing case in the context of protein dynamics in general, and the structure−function relationship associated with domain motions in enzymes (*15*), in particular. AKeco consists of a single 23.6-kDa polypeptide chain folded into domains CORE, AMPbd, and LID. It catalyzes the phosphoryl transfer reaction Mg^{2+}ATP + AMP ↔ Mg^{2+}ADP + ADP (*16*). The ribbon diagram of the "open" ligand-free form crystal structure (*17*) is shown in Figure 1a. CORE is the largest domain. It includes residues 1−29, 60−121, and 160−214, which form a five-stranded parallel β-sheet comprising strands $\beta_1-\beta_4$ and β_9 surrounded by helices α_1 and $\alpha_4-\alpha_9$. Domain AMPbd includes helices α_2 and α_3 formed by residues 30−59. The LID domain includes residues 122−159, which form a four-stranded antiparallel β-sheet (strands $\beta_5-\beta_8$). Domains AMPbd and LID are displaced significantly upon substrate binding (*17*−*20*). The

† This work was supported by the Israel Science Foundation Grant No. 520/99-16.1 to E.M., the Damadian Center for Magnetic Resonance Research at Bar-Ilan University, and an NIH/NCRR grant to J.H.F.

* Corresponding authors: E.M.: E-mail: eva@nmrsgi1.ls.biu.ac.il. Phone: 972-3-5318049. Fax: 972-3-5351824. J.H.F.: E-mail: jhf@ccmr.cornell.edu. Phone: 607-255-3647. Fax: 607-255-0595.

‡ Bar-Ilan University.

§ Cornell University.

|| Present address: Department of Medical Genetics and Microbiology, Faculty of Medicine, University of Toronto, Toronto, Ontario, Canada.

[1] Abbreviations: AK, adenylate kinase; AKeco, adenylate kinase from *Escherichia coli*; ATP, adenosine triphosphate; ADP, adenosine diphosphate; AMP, adenosine monophosphate; AMPbd, AMP-binding domain; AP_5A, P^1,P^5-di(adenosine-5′)pentaphosphate; CSA, chemical shift anisotropy; MF, model-free; NMR, nuclear magnetic resonance; NOE, nuclear Overhauser enhancement; SRLS, slowly relaxing local structure; VALM, very anisotropic local motion.

10.1021/bi012132q CCC: $22.00
Published on Web 04/24/2002

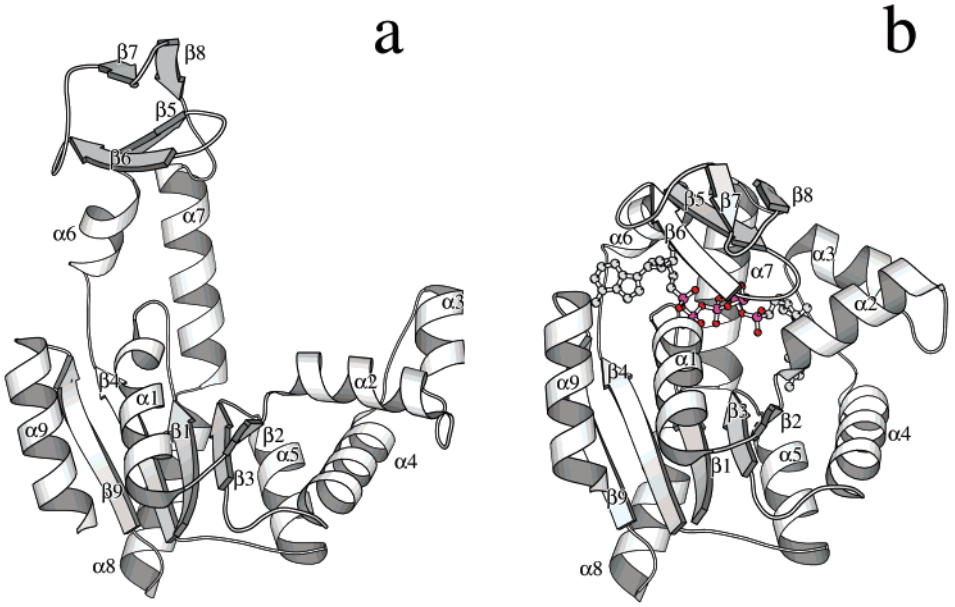

FIGURE 1: Ribbon diagram of the crystal structures of (a) AKeco and (b) AKeco in complex with the two-substrate-mimic inhibitor AP_5A. The figures were drawn with the program Molscript (*63*) using the PDB coordinate files 4ake (complex II) for AKeco and 1ake (complex II) for AKeco*AP_5A.

active site is configured thereby, and the "closed" structure, illustrated in Figure 1b by the ribbon diagram of the complex of AKeco with the two-substrate-mimic inhibitor AP_5A (*21*), is obtained. It is assumed that following the reaction the structure "opens up" again through reverse movements of AMPbd and LID to recover the original ligand-free enzyme (*17*). This mechanism has been inferred based on the crystal structures of ligand-free AK enzymes, and various molecular complexes with nucleoside monophosphates, nucleoside triphosphates, and inhibitors (*19*, *22*). Time-resolved fluorescence energy transfer studies of fluorescent AKeco derivatives confirmed domain closure in solution upon inhibitor binding (*23*, *24*). These studies also indicated that large-amplitude segmental mobility of AMPbd and LID is in effect in the ligand-free form (*23*). AKeco is the only adenylate kinase for which crystal structures corresponding to the extreme stages of the catalytic cycle are available (*17*, *21*, *22*), with the closed form represented by AKeco*AP_5A. The ATP phosphates are bound to the enzyme partly through the so-called P-loop GXXGXGK (residues 7−13). This binding motif between proteins and nucleotides occurs in many proteins that bind nucleoside triphosphates, in all the nucleoside monophosphate kinases, and in the weakly homologous G-proteins (*17*). When bound to AKeco, the two-substrate mimicking inhibitor AP_5A adopts a conformation close to the suggested transition state (*25*). Thus, we have at hand a prototype for a multidomain biological machine where mobility and function must be necessarily related. The SRLS concept of coupling between motions occurring on arbitrary time scales is particularly important for elucidating dynamic properties of proteins when segmental mobility is in effect.

Experimental ^{15}N relaxation data of AKeco and AKeco*-AP_5A acquired at 14.1 T were studied previously (*26*) using the conventional MF approach. The SRLS approach was applied recently to AKeco data acquired at magnetic fields of 14.1 and 18.89 T (*14*). This study indicated that SRLS is significantly more accurate and discriminating than MF. Herein we apply SRLS to AKeco*AP_5A, complementing the relaxation data acquired at 14.1 T (*26*) with ^{15}N T_1, T_2, and ^{15}N-{^1H} NOE data acquired at 18.79 T. The dynamic properties of the inhibitor-bound form were found to differ significantly from those of the ligand-free form. In general, two different dynamic models are experienced. These include the conventional rigid structure with rapid N−H bond fluctuations model, and a new intrinsically flexible model, where peptide planes move on the nanosecond time scale. The CORE domain of AKeco, and the majority of the AKeco*AP_5A residues, comply with the conventional model. It was found that the catalysis-related domains AMPbd and LID of AKeco are engaged in collective nanosecond peptide-plane motion interpretable as domain motion, and microsecond−millisecond conformational exchange. Residues within the loops β_1/α_1, α_2/α_3, α_4/b_3, α_5/β_4, and β_8/α_7 of AKeco*AP_5A experience nanosecond peptide plane motion which may be of a loop-swinging type. Loops α_4/β_3 and α_5/β_4 are rigid in AKeco and representative residues thereof are intrinsically flexible in AKeco*AP_5A, in accordance with the "energetic counterweight balancing of substrate binding" concept (*17*, *26*).

THEORETICAL BACKGROUND

We showed recently (*7*) that the two-body structural mode-coupling SRLS theory (*8*, *9*), extended in recent years to spin-labeled proteins (*10*−*12*), can also be applied to N−H bond vector motions in proteins. A short description of fundamentals is presented below.

The N−H bond vector and the protein surroundings (the two "bodies") are dynamically coupled by a potential $U(\Omega_{CM})$ that depends on their relative orientation $\Omega_{CM}(t)$, where C denotes the global diffusion frame of the protein surroundings, and M denotes the local diffusion/local ordering frame of the N−H bond vector. The local coupling potential exerted by the protein surroundings tends to align the N−H bond vector along the principal axes of the ordering frame. In the case of axially symmetric (along Z_M) local

ordering it is most simply given by (*10*−*12*):

$$U(\Omega_{CM})/k_BT = -c_{20}D^2{}_{00}(\Omega_{CM}) \quad (1)$$

where k_B is the Boltzmann constant, T is the temperature in K, c_{20} is the potential strength in units of k_BT, and $D^2{}_{00}$ is the Wigner rotation matrix element. A conventional order parameter can be related to c_{20} as (*10*):

$$S_{SRLS} = <D^2{}_{00}[\Omega_{CM}(t)]> \quad (2)$$

where the brackets imply ensemble averaging using the probability distribution based on the potential function given in eq 1 (*7*).

The time-dependent part of the spin Hamiltonian for this two-body system was given previously (*10*, *27*). The dynamic effects associated with the global and the local diffusion are incorporated into the spectral density through the diffusion operator (*9*, *10*):

$$\hat{\Gamma} = \hat{\Gamma}^{global}(\Omega_{LC}) + \hat{\Gamma}^{local}(\Omega_{LM}) + F^{global}(-\Omega_{CM}) + F^{local}(-\Omega_{CM}) \quad (3)$$

where L denotes the fixed laboratory frame. The first two terms in this equation refer to the freely globally diffusing protein surroundings and locally diffusing N−H bond vector, respectively. The last two terms reflect the contributions to $\hat{\Gamma}$ due to the potential $U(\Omega_{CM})$, which couples the global and local motions. F^{global} and F^{local} are functions of the Euler angles Ω_{CM} that transform the M frame into the C frame. This constitutes an effective two-body model for which a Smoluchowski equation representing the rotational diffusion of two interacting rotors is solved (*8*, *9*). The solution features three eigenvalues (correlation times) for the local motion when $S^2 = 0$:

$$(\tau_K)^{-1} = 6R^L{}_\perp + K^2(R^L{}_{||} - R^L{}_\perp) \text{ for } K = 0; 1; 2 \quad (4)$$

Each K value leads to its own spectral density component (*28*). For $S^2 > 0$ the $j_{K=0}(\omega)$ term represents mixed modes between the global motion, R^C, and the local motion component, $R^L{}_\perp$. When $R^L > R^C$ the $j_{K=1}(\omega)$ and $j_{K=2}(\omega)$ terms are dominated by $R^L{}_{||}$ and $R^L{}_\perp$, given in eq 4. The "measurable" spectral density is then constructed out of the three $j_K(\omega)$ components by incorporation of the orientation dependent functions that multiply the spin operators in the spin Hamiltonian (*28*).

Assuming that the ^{15}N CSA tensor is axially symmetric and collinear with the dipolar N−H tensor, the spectral density for ^{15}N CSA and ^{15}N-{^{1}H} dipolar relaxation in the coordinate frame of the local motion is given by (*28*, *29*):

$$J(\omega) = Aj_{K=0}(\omega) + Bj_{K=1}(\omega) + Cj_{K=2}(\omega) \quad (5)$$

where $A = (1.5\cos^2\beta_{MD} - 0.5)^2$, $B = 3\sin^2\beta_{MD}\cos^2\beta_{MD}$, $C = 0.75\sin^4\beta_{MD}$, and β_{MD} is the "diffusion tilt" angle between the molecular diffusion axis Z_M and the N−H bond vector. In the present study, the SRLS parameters featured by $J(\omega)$ include three diffusion rate constants: R^C (related to the global diffusion tensor), $R^L{}_\perp$ and $R^L{}_{||}$ (related to the local diffusion tensor), one potential parameter c_{20}, and the polar angle β_{MD} (diffusion tilt angle). Special cases include: (i) isotropic fast local diffusion (local correlation time $\tau_f \equiv \tau_\perp = (6R^L{}_\perp)^{-1} \approx \tau_{||} = (6R^L{}_{||})^{-1}$), implying $\beta_{MD} = 0$; then $J(\omega) = j_{K=0}(\omega)$, and the NMR relaxation data can be fit with one (c_{20}, if τ_f is negligibly small) or two (c_{20} and τ_f) free parameters, in formal analogy with the original MF spectral density (*4*, *5*), with τ_f denoting the local motion correlation time; (ii) very anisotropic slow local motion ($\tau_f \equiv \tau_{||} \ll \tau_s \equiv \tau_\perp$ and $\tau_f \rightarrow 0$), denoted VALM below; then the last two terms in eq 5 are negligibly small compared to $Aj_{K=0}$, provided $\beta_{MD} \neq 54.7°$, and NMR data can be reproduced with three free parameters (c_{20}, τ_s, β_{MD}). The VALM spectral density is formally analogous (*7*, *14*) to the reduced extended MF spectral density (*6*). If NMR data at more than one magnetic field are available, VALM can be extended by allowing $\tau_f \equiv \tau_{||}$ to be a free parameter. Then all the $j_K(\omega)$ components contribute to $J(\omega)$ in eq 5. For small β_{MD} angles, the SRLS spectral density is (given the above assumptions) formally analogous to the extended MF spectral density (*30*). The expression $(1.5\cos^2\beta_{MD} - 0.5)^2$ is formally analogous to S_f^2 (*7*, *14*).

The CSA spectral density can be corrected for non-collinearity of the ^{15}N CSA and ^{15}N−^{1}H dipolar tensors, which are tilted at an angle θ (*33*), by addition of ΔJ^{CSA} (*7*, *14*). As discussed previously (*7*, *14*), the angle γ_{MD} between the Y axis of the magnetic dipolar tensor and the Y axis of the M frame was set at 90°. In this case, the perpendicular local motion occurs about an axis (Y_M) lying in the peptide plane parallel to the $N_i-C_i^\alpha$ bond, or the $C_{i-1}^\alpha-C_i^\alpha$ axis.

After the spectral density function $J(\omega)$ has been constructed out of its fundamental $j_K(\omega)$ components using eq 5, the measurable ^{15}N relaxation quantities ^{15}N T_1, ^{15}N T_2, and ^{15}N-{^{1}H} NOEs are calculated as a function of $J(0)$, $J(\omega_N)$, $J(\omega_H)$, $J(\omega_H + \omega_N)$, and $J(\omega_H - \omega_N)$, using standard expressions for NMR spin relaxation (*3*, *34*).

The formal analogy between SRLS and MF spectral densities can be further clarified by giving the form of the expression for the SRLS $j_K(\omega)$ functions. The solution of the two-body Smoluchowski equation consists of eigenmodes $1/\tau_i$ and weighing factors c_i, such that $j(\omega) = \sum_i c_i\tau_i/(1 + \omega^2\tau_i^2)$. The eigenmodes $1/\tau_i$ represent pure or mixed dynamic modes, in accordance with the parameter range considered. For example, for $R^C/R^L = 0.01$ the global motion is given by the smallest eigenmode, with increasing weight as S^2 increases (Table 5 of ref *8*). The local motion is given by a large number of mixed eigenmodes with two (for $0.2 < S^2 < 0.5$) or one (above $S^2 = 0.5$) having weights comparable to that of the global motion eigenmode. Yet, the combined contribution of the (three or two) dominant eigenmodes to $j(\omega)$ in the noted S^2 range is only about 80%, with the rest contributed by a large number of large mixed eigenmodes with small individual weights. The SRLS function $J(\omega)$ is constructed out of the $j_K(\omega)$ components. The $J(\omega)$ from the SRLS approach we use (as described above) and from MF have similar general forms and feature the same number of free parameters (more sophisticated forms of SRLS are available as needed) (*7*, *10*). In this respect, they are "formally analogous" but not identical, because the MF $J(\omega)$ are not precisely the same dynamic modes and associated weights, nor does MF distinguish between the different $j_K(\omega)$ in eq 5. Identity is achieved only in the limiting cases where $J(\omega)$ for SRLS yields the MF formulas. We found that the contribution of mixed modes is on the order of typical experimental errors when S^2(SRLS) > 0.9 and τ(SRLS) <

Table 1: SRLS Models Used to Fit Experimental AKeco and AKeco*AP_5A ^{15}N NMR Relaxation Data Acquired at Two Magnetic Fields

no	parameters[a]	SRLS model description
1	c_{20}	very fast internal motion ($\tau \rightarrow 0$)[b]
2	c_{20} (S^2); $\tau(\tau_f)$	isotropic internal motion
3	c_{20} (S^2); R_{ex}	model 1 with exchange term
4	c_{20} (S^2); $\tau(\tau_f)$; R_{ex}	model 2 with exchange term
5	c_{20} (S_s^2); β_{MD} (S_f^2); $\tau_\perp(\tau_s)$	very anisotropic internal motion ($\tau_{\|} \rightarrow 0$)[c]
6	c_{20} (S_s^2); β_{MD} (S_f^2); $\tau_\perp(\tau_s)$; $\tau_{\|}(\tau_f)$	anisotropic internal motion[d]
7	c_{20} (S_s^2); β_{MD} (S_f^2); $\tau_\perp(\tau_s)$; R_{ex}	model 5 with exchange term
8	c_{20} (S_s^2); β_{MD} (S_f^2); $\tau_\perp(\tau_s)$; $\tau_{\|}(\tau_f)$; R_{ex}	model 6 with exchange term

[a] Analogous MF parameters are shown in parentheses. [b] For model 1, the $\tau \rightarrow 0$ assumption is practically equivalent to fixing τ at the lowest value for which the SRLS spectral densities could be calculated. [c] For model 5, the $\tau_{\|} \rightarrow 0$ assumption is equivalent to neglecting the $j_{K=1}(\omega)$ and $j_{K=2}(\omega)$ spectral density components. [d] For models 6 and 8, where in practice $\tau_{\|} \ll \tau_\perp$, $j_{K=1}(\omega)$, and $j_{K=2}(\omega)$ components calculated for an isotropic local diffusion tensor with correlation time $1/(6\ R^L{}_\perp)$ were used in eq 5.

40 ps. As indicated in ref *7*, and further demonstrated in this study, the MF limits are not precisely attained over the parameter range relevant to folded proteins. The parameter most sensitive to departures from these limits is τ.

The theory outlined above has been implemented in a fitting scheme (*7*). The SRLS-based dynamic models employed to fit the two-field ^{15}N relaxation data of AKeco are summarized in Table 1. In model 1, the local motion is so fast ($\tau_f \rightarrow 0$) that its effect on the spectral density is negligible. This assumption is equivalent in practice to fixing τ_f at the lowest value for which the SRLS spectral densities could be calculated. In model 2, it is assumed that the internal motion can be approximated as isotropic ($\tau_\perp = \tau_{\|}$). Models 3 and 4 are derived from models 1 and 2, respectively, by addition of the free parameter, R_{ex}, to the transverse relaxation rate expressions to account for exchange processes on the microsecond to millisecond time scales. For models $1-4$ $\beta_{MD} = 0$, hence $J(\omega) = j_{K=0}(\omega)$ in eq 5. In model 5 (VALM), the local motion is assumed to be very anisotropic, i.e., $\tau_f \equiv \tau_{\|} \ll \tau_s \equiv \tau_\perp$, and $\tau_f \rightarrow 0$. In this case, only $\tau_\perp$ enters the spectral density. The angle β_{MD} is allowed to vary, affecting $J(\omega)$ through the coefficient A in eq 5. In model 6, the restriction $\tau_{\|} \rightarrow 0$ is removed letting $\tau_{\|}$ be a free variable. The local motion (R^L) of an N$-$H bond restricted to the peptide plane is necessarily highly anisotropic (see below). It was found that in this limit $j_{K=1}(\omega)$ and $j_{K=2}(\omega)$ in eq 5 are well approximated by their counterparts calculated for an isotropic local diffusion tensor with correlation time $1/(6\ R^L{}_\perp)$. These approximations were used in models 6 and 8. Models 7 and 8 are derived from models 5 and 6, respectively, by addition of the free parameter R_{ex}.

MATERIALS AND METHODS

Sample Preparation. For preparation of uniformly ^{15}N-labeled AKeco, *Escherichia coli* HB101 cells transformed with the pEAK91 plasmid were grown at 37 °C in Celtone-N medium (Martek Biosciences Corp., US) containing >98% ^{15}N. The recombinant plasmid pEAK91 contained the intact gene coding for *E. coli* adenylate kinase (*35*). The previously described procedure for purification of AKeco (*24*) was improved by application of Blue-Sepharose affinity chromatography (*35*), followed by size-exclusion chromatography on a Sephacryl S-100 column (Pharmacia, Sweden). AKeco stock solution was prepared by thorough dialysis of the protein solution against 40 mM sodium phosphate buffer (pH 6.8) containing 10 μM sodium azide, followed by concentration on a Centricon-10 concentrator (Amicon, US). The concentration of the AKeco solution was determined based on the absorption coefficient $A_{277} = 0.5$ mg/mL^{-1} cm^{-1} (*36*). An appropriate amount of AP_5A (Boehringer, Germany) inhibitor stock solution (pH 6.8) and 50% D_2O, prepared in the same buffer, were added to the concentrated AKeco solution to obtain fully saturated enzyme in the AKeco*AP_5A sample. The ligand-free sample contained 1.75 mM ^{15}N-labeled enzyme and 40 mM sodium phosphate buffer in 95% H_2O/5% D_2O. The inhibitor-bound sample contained 2 mM ^{15}N-labeled enzyme, 2.5 mM AP_5A, and 40 mM sodium phosphate buffer in 95% H_2O/5% D_2O. The protein samples were degassed and transferred to 5-mm NMR Shigemi cells. Protein monodispersion was ascertained previously (*26*).

NMR Spectroscopy. NMR experiments were carried out at 303 K on Bruker DMX-600 and DRX-800 spectrometers operating at 14.1 and 18.79 T, respectively, using 5-mm ^1H-^{13}C-^{15}N triple resonance inverse detection probes and B-VT-2000 and BTO-2000 temperature control units at 14.1 and 18.79 T, respectively. NMR data were analyzed on Silicon Graphics workstations using the software packages nmrPipe and modelXY (*37*). The previously determined assignments of the AKeco ^1H-^{15}N correlations (*38*), complemented and revised in our earlier study (*26*), were used. The assignments of the AKeco*AP_5A ^1H-^{15}N correlations were taken from ref *39*.

Relaxation times T_1 and T_2, and NOE parameters were measured using established inversion recovery (*40*), spin$-$echo (*41*), and ^{15}N-{^1H} steady-state NOE (*42*) pulse sequences, as described in refs *43*$-$*45*. A 0.5-ms spin$-$echo period was used in the CPMG T_2 experiments. For NOE experiments, we used sequence 1B of ref *45*, which features H_2O flip-back pulses to minimize saturation of water. Spectral widths were 1824.5 and 2432.6 Hz in the F_1 dimension, and 9615.4 and 12820.5 Hz in the F_2 dimension at 14.1 and 18.79 T, respectively. The ^{15}N carrier was set at 117.5 ppm and was referenced indirectly to liquid NH_3 (*46*). 360×2048 complex points were acquired in the $t_1 \times t_2$ dimensions for each time point.

The ^{15}N T_1 and T_2 measurements were performed using a total of 40 and 64 transients per t_1 experiment, respectively. For the T_1 measurements of AKeco, nine time points were collected using parametric delays of 15, 127, 247, 367, 487, 647, 807, 1031, and 1287 ms at 14.1 T, and 15, 127, 327, 567, 807, 1047, 1367, 1767, and 2247 ms at 18.79 T. The experiment was repeated twice for time points 15, 487, and 1287 ms at 14.1 T, and 15, 807, and 2247 ms at 18.79 T. The delay between scans was set to 1.5 s at 14.1 T and 2 s at 18.79 T. For the T_1 measurements of AKeco*AP_5A, eight time points were collected using parametric delays of 133.5, 245.5, 357.5, 485.5, 645.5, 805.5, 997.5, and 1285.5 ms at 14.1 T, and nine time points were collected using parametric delays of 15, 127, 327, 567, 807, 1047, 1287, 1607, and 2007 ms at 18.79 T. The experiment was repeated twice for each

time point at 14.1 T, and for 15, 807, and 2007 ms at 18.79 T. The delay between scans was set to 1.5 s at 14.1 T and 2.2 s at 18.79 T for both AKeco forms. For the T_2 measurements of AKeco, nine time points were collected using parametric delays of 8, 16, 24, 32, 48, 64, 80, 96, and 128 ms at 14.1 T, and eight time points were collected using parametric delays of 8, 16, 32, 48, 64, 80, 104, 128 ms at 18.79 T. The experiment was repeated twice for time points 8, 64, and 128 ms. For the T_2 measurements of AKeco*AP_5A, nine time points were collected using parametric delays of 8, 16, 24, 32, 48, 64, 80, 96, and 128 ms at 14.1 T, and eight time points were collected using parametric delays of 8, 16, 32, 48, 64, 80, 104, and 128 ms at 18.79 T. The experiment was repeated twice for time points 8, 24, 64, and 128 ms at 14.1 T, and 8 and 48 ms at 18.79 T. The delay between scans was set to 1.6 s at 14.1 T and 1.9 s at 18.79 T for both AKeco forms. The data were apodized with a cosine (cosine-bell) window function in t_1 (t_2). Duplicates were used to calculate average values of, and uncertainties in, the measured peak heights. Phenomenological T_1 and T_2 values and uncertainties were determined by nonlinear least-squares fitting of the experimental data to monoexponential equations (*47*).

The ^{15}N-{^{1}H} NOE values were measured using pairs of spectra recorded in an interleaved mode with and without proton presaturation during the recycle delay. A total of 96 transients per t_1 experiment were recorded. The delay between scans was 3.8 and 6.6 s for AKeco and 3.8, 6.6, or 12.1 s for AKeco*AP_5A at 14.1 T, and 5.4 s for AKeco and 5.7 s for AKeco*AP_5A at 18.79 T. The data were processed as described above. The ^{15}N-{^{1}H} NOE values were recorded in duplicate, and the replicates were used to determine uncertainties and mean values.

Data Analysis. The calculation of SRLS spectral densities is computationally intensive for c_{20} values exceeding ~10 (S^2 exceeding ~0.81) and/or very fast internal motions. Therefore, in adapting SRLS to protein relaxation analysis we used precalculated[2] two-dimensional grids of $j(0)$, $j(\omega_N)$, $j(\omega_H)$, $j(\omega_H + \omega_N)$, and $j(\omega_H - \omega_N)$ to fit experimental ^{15}N T_1, T_2, and ^{15}N-{^{1}H} NOE data. (*7*) The $j_{K=0}$, $j_{K=1}$, and $j_{K=2}$ grids of spectral density values at the five frequencies were constructed under the assumption of isotropic global motion for sets of c_{20} and τ_f (or τ_s) values. An axial ^{15}N chemical shielding tensor with $\sigma_{||} - \sigma_\perp = -170$ ppm, $r_{NH} = 1.02$ Å, and $\theta = -16°$ (e.g., see ref *48*) were used in these calculations. The c_{20} grid dimension spanned the values between 0 ($S^2 = 0$) and 40 ($S^2 = 0.95$), and the τ dimension spanned the values between $0.0005\tau_m$ and $1.4\tau_m$. The ratio τ/τ_m was interpolated to 0 as required. A two-dimensional polynomial interpolation using Neville's algorithm (*49*) was employed for spectral density evaluation in the course of model fitting. The interpolation errors in both the c_{20} and τ grid dimensions were estimated to be at least one order of magnitude smaller than the errors in the fitted microdynamic parameters. The fitting of experimental NMR data was based on Powell minimization (*49*) of a target function. The target function for spin i was defined as the sum of the squared differences between experimental and calculated T_1, T_2, and ^{15}N-{^{1}H} NOE values divided by the squared random errors:

$$\chi^2_i = \sum[(T_{1i}^{obs} - T_{1i}^{calc})/\sigma_{T1,i}]^2 + [(T_{2i}^{obs} - T_{2i}^{calc})/\sigma_{T2,i}]^2 + [(NOE_i^{obs} - NOE_i^{calc})/\sigma_{NOEi}]^2 \quad (6)$$

where the sum runs over the magnetic fields used in acquiring the experimental data. The model selection scheme employed in the fitting program was based on χ^2- and F-statistic testing and followed closely the schemes used for MF analysis, as described previously (*7*). Errors in microdynamic parameters were evaluated based on Monte Carlo simulations (*50*) using 100 randomly distributed synthetic data sets. Convergence was ascertained by obtaining practically identical results with a larger number of Monte Carlo simulations in representative calculations.

The fundamentals of the MF calculations were described earlier (*51*), and the details of their application to the AKeco and AKeco*AP_5A data acquired at 14.1 T were given previously (*26*).

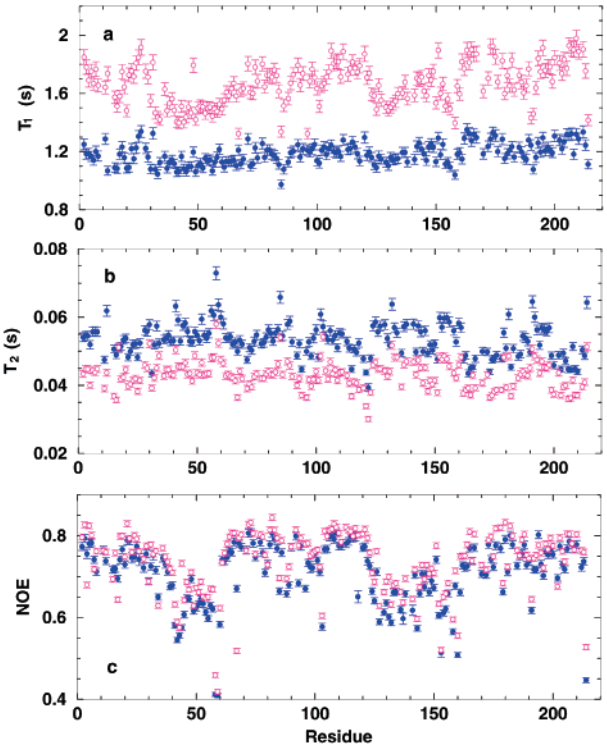

FIGURE 2: Experimental relaxation parameters of AKeco (a) ^{15}N T_1, (b) ^{15}N T_2, and (c) ^{15}N-{^{1}H} NOE derived from data acquired at 303 K at 14.1 T (solid circles) and 18.79 T (opaque circles) as a function of residue number.

RESULTS AND DISCUSSION

The experimental ^{15}N T_1, T_2, and ^{15}N-{^{1}H} NOE data, acquired at 14.1 and 18.79 T for AKeco are shown in Figure 2. It can be seen that the ^{15}N-{^{1}H} NOE is the most sensitive parameter, with NOE values clearly reduced in the chain regions corresponding to domains AMPbd and LID. T_1 values are lower within AMPbd and within the LID chain segment extending from residue G122 to residue F137. The experimental ^{15}N T_1, T_2, and ^{15}N-{^{1}H} NOE data, acquired at 14.1 and 18.79 T for AKeco*AP_5A, are shown in Figure 3. NOE

[2] Following the publication of ref *7*, we detected a small error in the j(ω) computations. In general, the dynamical picture, the results of the SRLS fitting, and our conclusions did not change. In particular, discrepancies of several percent between SRLS and MF in Figures 3a, 4a, 4c, 5a, and 6a, in the limit when they are expected to become equal, have now been removed.

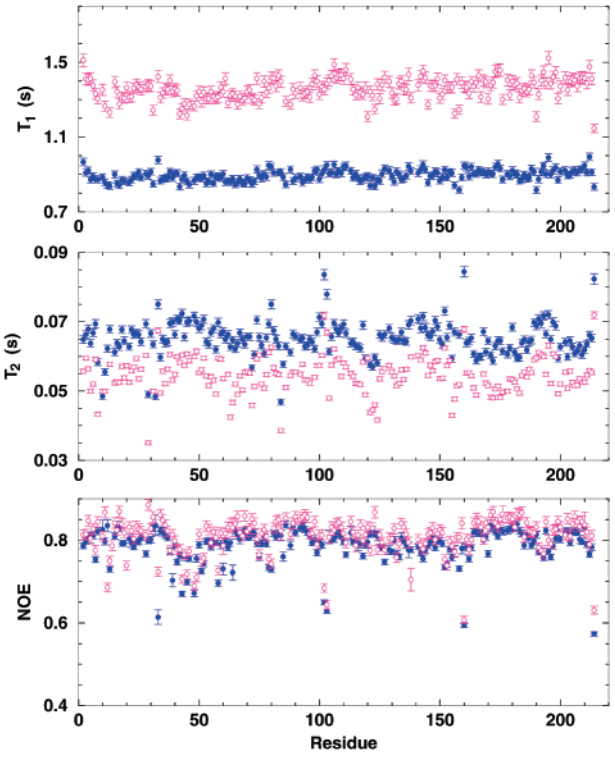

FIGURE 3: Experimental relaxation parameters of AKeco*AP$_5$A (a) ^{15}N T_1, (b) ^{15}N T_2, and (c) ^{15}N-{^{1}H} NOE derived from data acquired at 303 K at 14.1 T (solid circles) and 18.79 T (opaque circles) as a function of residue number.

values acquired at both 14.1 and 18.79 T are reduced within loop α_2/α_3 of domain AMPbd, loops α_4/β_3 and α_5/β_4 of CORE, and residues Q160 and G214. The T_1 and T_2 profiles display limited variability. The NOE and T_2 values are on average smaller, and the T_1 values larger, for the ligand-free enzyme, pointing qualitatively to a larger and more flexible particle prevailing in solution in the absence of inhibitor.

The combined data sets featuring 188 residues for AKeco and 187 residues for AKeco*AP$_5$A were subjected to SRLS analysis, with the experimental errors on average 2.5% for AKeco and 3.5% for AKeco*AP$_5$A. The χ^2 probability confidence level was set at 5% (in a few cases at 1%), and the F-statistic probability confidence level at 20%. With these criteria, the experimental data of 86% of the AKeco residues, and 96% of the AKeco*AP$_5$A residues, could be fit.

Global Diffusion. Domains AMPbd and LID of AKeco execute in solution large-amplitude segmental motions (*23*, *24*). On the NMR time scale, conformational averaging leads to a well-defined average structure (*26*). A detailed discussion of its global diffusion tensor, R^C, was presented previously (*14*). It was concluded that isotropic diffusion with $\tau_m = 15.1 \pm 0.1$ ns constitutes an appropriate approximation, with the provision that exchange contributions beyond Q160 may also reflect geometric features associated with R^C anisotropy (*26*). The inhibitor-bound complex is quite rigid and similar to the nearly spherical crystal structure (*26*, *52*). Therefore, it lends itself particularly well to global diffusion tensor determination based on the quadratic approximation (*53*, *54*). This has been accomplished previously (*26*) to yield τ_m(app) $= 11.6 \pm 0.1$ ns and a diffusion anisotropy $D_{||}/D_\perp = 1.11$. The quadratic approximation (*53*) makes possible calculating (*54*) effective correlation times $\tau_m(i)$ for each residue *i*. Using these $\tau_m(i)$ values led to practically the same results as using $\tau_m = 11.6 \pm 0.1$ ns, with the same provision in regards with R_{ex} terms beyond Q160 as mentioned above for AKeco. On the basis of these considerations, $\tau_m = 11.6$ ns was used in all further calculations.

Local Motion. The combined two-field data sets of AKeco and AKeco*AP$_5$A were subjected to SRLS fitting (*7*) using the eight SRLS models (Table 1), which can be classified into the simplified models 1−4 and the somewhat more general models 5−8. In the first model category, it was assumed that R^L is in the extreme motional narrowing limit (models 1 and 3) or isotropic (models 2 and 4). The latter simplification is justified when the time scale separation between R^L and R^C is large, as in this case $j_{K=0}(\omega)$ is dominated by the global diffusion, and determining R^L with reasonable accuracy is difficult. The model 5−8 category includes general cases of weaker coupling potentials and smaller time scale separations, when the tensor R^L must be at least axially symmetric. Since $R^L \gg R^C$ for models 1−4 and $R^L{}_\perp = R^C$ for models 5−8, we denote the former parameter range as the "ps regime", and the latter parameter range as the "ns regime". With AKeco the majority of the CORE residues were associated with the ps regime and fit with models 2 and 4. The AMPbd and LID residues were associated with the ns regime and fit with models 6 and 8. With AKeco*AP$_5$A loop α_2/α_3, and representative residues of loops β_1/α_1, α_4/β_3, α_5/β_4, and β_8/α_7, were associated with the ns regime and fit mostly with model 6. The rest of the backbone was associated with the ps regime and fit with models 1−4, pointing out outstanding rigidity.

The best-fit microdynamic parameters obtained with the SRLS analysis are depicted in Figures 4 and 5. The squared order parameters, S^2, are clustered into two distinct narrow ranges. With AKeco $S^2 = 0.78-0.90$ in the ps regime and 0.18−0.49 in the ns regime, and with AKeco*AP$_5$A $S^2 = 0.82-0.95$ in the ps regime and 0.15−0.38 in the ns regime (Figure 4a). The local motion correlation times $\tau_{||}$ are shown in Figure 4b. Note that with models 2 and 4 this parameter represents the presumed isotropic correlation time $\tau \equiv \tau_{||} \approx \tau_\perp$. This assumption appears to be justified by τ/τ_m of $(0.3-8.7) \times 10^{-3}$ for AKeco and $(0.4-16.0) \times 10^{-3}$ for AKeco*AP$_5$A. With models 6 and 8, $\tau_{||}$ represents the parallel component of the axial local diffusion tensor R^L, on the order of 5 ps for AKeco and 11−31 ps for AKeco*AP$_5$A. The perpendicular component $\tau_\perp$ of R^L, shown in Figure 4c, spans the range of 5.7−11.3 ns for AKeco and 5.6−9.6 ns (one outlier A11 with $\tau_\perp = 10.7$ ns) for AKeco*AP$_5$A.

The R_{ex} data appear in Figure 4d. The issue of experimental confirmation of the best-fit R_{ex} terms was addressed previously (*14*). On the basis of $T_{1\rho}$ experiments (*55*), the measurement of cross-correlated ^{15}N CSA−^{15}N−^{1}H dipolar relaxation rates η_{xy} (*56*), numerical simulations and general considerations (*14*), and the current AKeco*AP$_5$A data, the following results were obtained. Within AMPbd and LID of AKeco R_{ex} lies largely between 2.3 and 4.4 s^{-1} and is likely to represent genuine conformational exchange (*14*). It is reduced mostly below 2 s^{-1} in the LID domain (two outliers T155 with $R_{ex} = 3.9$ s^{-1}, and R156 with $R_{ex} = 6.1$ s^{-1}), and largely suppressed in the AMPbd domain upon inhibitor binding, in accordance with domain motion being discontinued. For both enzyme forms R_{ex} terms within CORE below Q160 are likely to represent genuine exchange (*14*).

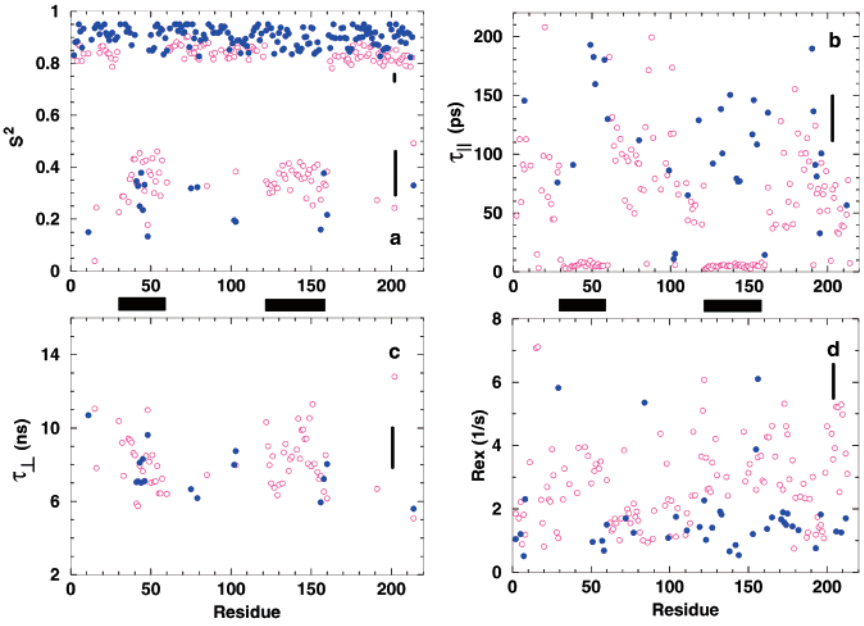

FIGURE 4: Best fit microdynamic parameters obtained by applying SRLS to the combined data of AKeco (opaque magenta circles) and AKeco*AP$_5$A (solid blue circles): (a) squared order parameter, S^2; (b) parallel SRLS local motion correlation time component $\tau_{||}$ (τ_f); (c) perpendicular SRLS local motion correlation time component $\tau_\perp$ (τ_s), and (d) exchange term, 14.1 T R_{ex}, plotted as a function of residue number. For SRLS models 5−8, the squared order parameter, S^2, is calculated as the product of S_{SRLS}^2 and $(1.5\cos^2\beta_{MD} - 0.5)^2$, where S_{SRLS} is equivalent to S_s and $(1.5\cos^2\beta_{MD} - 0.5)$ to S_f in the extended MF formula. Average errors for both enzyme forms are given as solid bars on the right-hand side of each Figure. Individual errors are given in the Supporting Information. The black boxes represent the domains AMPbd and LID. Data were taken from Tables S3 and S4 of the Supporting Information.

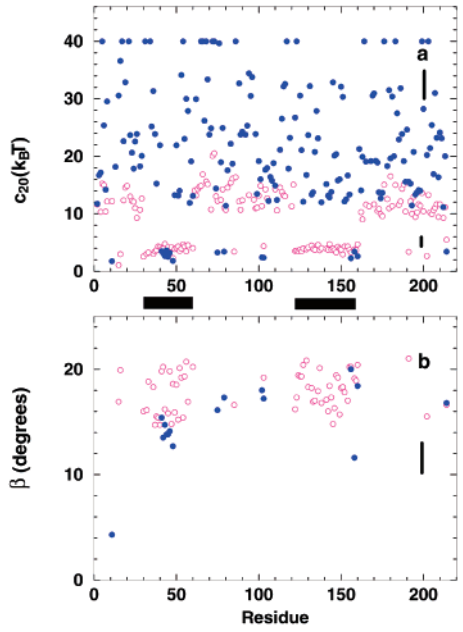

FIGURE 5: As in the captions of Figure 4 for (a) the coupling potential coefficient c_{20} (eq 1) corresponding to S_{SRLS} (eq 2), and (b) the tilt angle β_{MD} between the collinear local diffusion and ordering axes and the principal axis of the magnetic dipolar tensor, plotted as a function of residue number. Average errors for both enzyme forms are given as solid bars on the right-hand side of each figure. Individual errors are given in the Supporting Information. The black boxes represent the domains AMPbd and LID. Data were taken from Tables S3 and S4 of the Supporting Information.

The AKeco*AP$_5$A residues associated with outstandingly large R_{ex} terms include I29, D84, T155, and R156.

The best-fit values of the coefficient c_{20}, which gauges directly the strength of the coupling potential (eq 1) associated with the order parameter S_{SRLS} (eq 2), are shown in Figure 5a. With AKeco $c_{20} = 9.0-20.5\ k_BT$ in the ps regime and $2.3-4.7\ k_BT$ in the ns regime. With AKeco*AP$_5$A $c_{20} = 11.4-40.0\ k_BT$ in the ps regime, and $1.8-3.8\ k_BT$ in the ns regime. The angle β_{MD} between the local diffusion/ordering axis and the N−H bond assumes values of 14.7−21.0° for AKeco and 11.6−20.0° for AKeco*AP$_5$A in the ns regime.

Validity Range of the MF Limit. The SRLS spectral density is expected to yield the MF spectral density as $\tau_f \rightarrow 0$. The range of τ_f values wherein SRLS and MF $J(\omega)$ can be considered to be practically identical is determined by the experimental error, ω and S^2. These ranges can be determined theoretically by simulating T_1, T_2, and NOE with SRLS and MF. We carried out such calculations using analogous microdynamic parameters, evaluated relative percentage errors, and considered convergence of SRLS $J(\omega)$ to the MF asymptote practically achieved if these data were comparable to the experimental errors. AKeco*AP$_5$A turned out to be an exceptionally rigid molecular complex featuring a large number of residues fit with model 1, where $\tau_f = 0$, and model 2, where τ_f is small. This enabled assessing MF validity on the level of data fitting, besides theoretical simulations. The AKeco*AP$_5$A data were subjected to MF fitting using the program DYNAMICS (*57*), and corresponding microdynamic parameters were compared for residues where both SRLS and MF selected model 1 or model 2. Relative percentage errors were evaluated, considering convergence of SRLS to MF practically achieved if these data were comparable to the Monte Carlo errors determined by the fitting process. Both simulation and data fitting indicated that SRLS $J(\omega)$ converges to MF $J(\omega)$ for $\tau_f = 0$. For finite values of τ_f, we found with simulations that the relative percentage errors in T_1, T_2, and NOE remain below approximately 2% up to 7 (75) ps for $S^2 = 0.8$ (0.95), for magnetic fields of

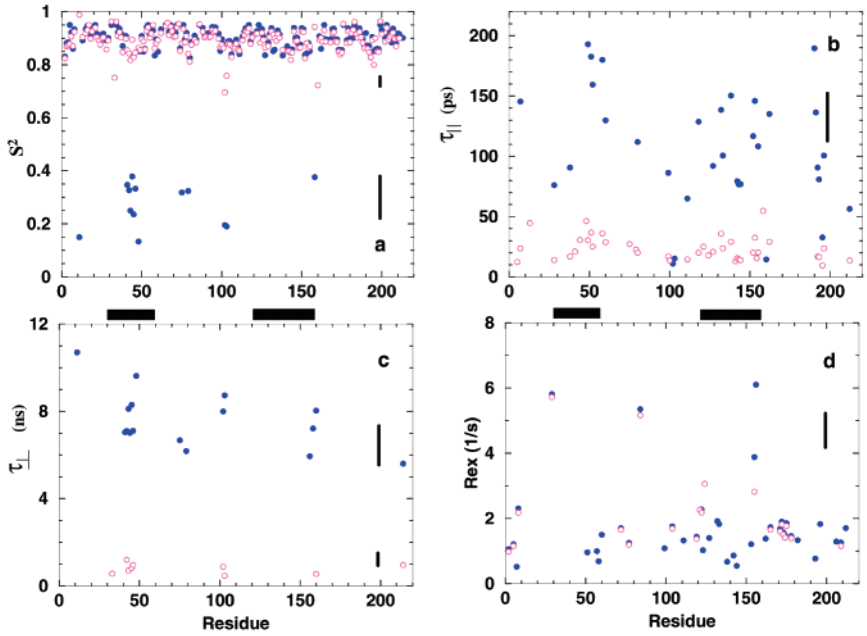

FIGURE 6: Best fit microdynamic parameters for AKeco*AP$_5$A obtained by applying SRLS (solid blue circle) and MF (opaque magenta circles) to the combined data set: (a) squared order parameter, S^2; (b) parallel SRLS local motion correlation time component $\tau_{||}$ (τ_f in MF); (c) perpendicular SRLS local motion correlation time component $\tau_\perp$ (τ_s in MF); and (d) exchange term, 14.1 T R_{ex}, plotted as a function of residue number. Average errors for both enzyme forms are given as solid bars on the right-hand side of each figure. Individual errors are given in the Supporting Information. The black boxes represent the domains AMPbd and LID. Data were taken from Tables S4 and S5 of the Supporting Information.

14.1 and 18.8 T. These simulations also indicated that T_1 and T_2 are much less sensitive than the NOE to increasing values of τ_f. Model 2 fittings gave comparable SRLS and MF S^2, and MF τ_f smaller on average by a factor of 4 than SRLS τ_f. This is in accordance with the simulations, as for larger proteins T_1 and T_2 constitute the major determinants of S^2, while the *NOE* is the major determinant of τ_f. The data given above constitute quantitative assessments of MF validity. They are relevant to MF aspects such as determination of the global diffusion tensor (*54*, *58*), applicability of the simplified expressions for cross-correlated spectral densities (*59*), the model-independent approach (*56*), etc.

Physical Models. The ps regime and ns regime models have been described in detail previously (*14*). A brief summary will be provided below for convenience. The ps regime model features S^2 and τ_f as SRLS variables, with the former high and the latter low. It represents the conventional model of a rigid protein structure with rapid small amplitude fluctuations about the equilibrium N−H bond orientation. The ns regime model features S^2, $\tau_{||}$, $\tau_\perp$, and β_{MD} as SRLS variables. In the ns regime, the SRLS fitting gave typically low parallel Z_M ordering. This is still consistent with large perpendicular (negative) Y_M ordering and Z_M ordering (currently determined to be approximately $S^2 = 0.3$) higher than X_M ordering (*32*). The rigorous approach is to add the rhombic term in eq 1, and carry out the SRLS fitting for an asymmetric ordering tensor. On the basis of data fitting Y_M lies within the peptide plane perpendicular to Z_M, which is tilted out-of-plane at approximately 20° from the N−H bond, and $\tau_{||} \ll \tau_\perp$. This is consistent with the N−H orientations motionally averaged by $\tau_{||}$ about Z_M, and the average Z_M axis reorienting about Y_M with correlation time $\tau_\perp$. The $\tau_\perp$ mode is on the ns time scale defined by the global diffusion correlation time, τ_m. The angle β_{MD} is on the order of 20°, in compliance with Y_M being aligned close to the $C^\alpha_{i-1}-C^\alpha_i$ axis (*60*). The angle H−N−C$^\alpha$ of 113° (ref *61*) renders Y_M parallel to the $N_i-C^\alpha_i$ bond also geometrically feasible. The specific values of the various parameters converge to the physical picture of nanosecond peptide plane motion. With AKeco the conspicuous parameter clustering is suggestive of collective ns motions interpretable as domain motion. AKeco*AP$_5$A does not experience domain mobility and the ns motions may be of a loop-swinging type. Higher accuracy in model characterization will be achieved after implementing asymmetric ordering (*14*). The latter feature is also expected to have implications to the interpretation of order parameters in terms of fast asymmetric local motions (*60*).

Comparison between SRLS and MF Analyses. A detailed account of the results obtained with SRLS and MF for the ligand-free enzyme is given in ref *14*. The main results obtained for the ps regime CORE domain, and the ns regime AMPbd/LID domains, are summarized below for convenience. In the ps regime, MF S^2 is mostly higher than SRLS S^2, in excess of the experimental error. In some cases, they are practically the same. The MF τ_f value ranges between 5 and 50 ps, while its SRLS counterpart ranges mostly between 5 and 131 ps. Analysis of corresponding pairs indicated that MF underestimates local motion correlation times by factors of 3−6. In the ns regime, MF S^2 overestimates SRLS S^2 on average by 131%, rendering the S^2 profile quite insensitive to the distinction between ps regime and ns regime dynamics. The MF profiles of τ_f and τ_s do single out AMPbd and LID qualitatively, but the quantitative differences are substantial, with MF τ_s underestimating SRLS $\tau_\perp$ on average by a factor of 11.

The best-fit parameters obtained with SRLS for the inhibitor-bound enzyme are shown in Figure 6 superimposed on the best-fit parameters obtained with MF. Most residues pertain to the ps regime, where the S^2 values obtained with SRLS and MF are comparable, with $<S^2> = 0.9$ (Figure

6a). The average MF τ_f value is 25 ps, and the average SRLS $\tau_{||}$ value is 125 ps. Analysis of corresponding pairs indicated that MF underestimates this parameter by factors of 4.5−9 (Figure 6b). SRLS identifies loops β_1/α_1, α_2/α_3, α_4/β_3, α_5/β_4, and β_8/α_7 as flexible, by associating representative residues thereof with ns regime dynamics. The pertinent parameters were determined as $<S^2> = 0.3$ (Figure 6a) and $<\tau_\perp> = 7.6$ ns (Figure 6c). MF only identifies loops α_5/β_4 and β_8/α_7 as flexible, with $<S^2> = 0.73$ and $<\tau_\perp> = 0.8$ ns. Thus, for slow local motions, MF overestimates $<S^2>$ by 143% and underestimates $<\tau_\perp>$ by a factor of 9.5. When SRLS and MF identify R_{ex} terms for the same residue, the magnitudes are mostly comparable (Figure 6d). SRLS identifies several additional R_{ex} terms typically below 2 s^{-1}, except for the R_{ex} contributions of residues T155 and R156.

It is concluded that the dynamic picture provided by SRLS is significantly more accurate and discriminating than the dynamic picture provided by MF. The well-defined meaning of the SRLS parameters, notably, the interpretation of $<\tau_\perp>$ of AKeco as correlation time for domain motion (*14*), provides new physical insight. MF can mostly determine satisfactorily axial order parameters in the ps regime.

Relation between SRLS Dynamics and the Mechanics of E. coli AKeco Catalysis. AKeco catalysis takes place through movements of the domains AMPbd and LID. With the ligand-free enzyme, ps regime dynamics is associated with the structural scaffold CORE (*21*), and ns dynamics with the segmentally mobile domains (*23*, *24*) AMPbd and LID (*14*). The tightly clustered ns regime parameters concur to a dynamic model where $<\tau_\perp>$ represents the correlation time for domain motion, found to be on the order of nanoseconds (*14*). To our knowledge, this is the first direct measurement of domain motion correlation time. This is very significant for understanding kinase catalysis. On the basis of the rationale outlined above for AKeco, the entire backbone of AKeco*AP_5A is expected to feature ps regime dynamics. Therefore, the regions of interest are the ns regime loops β_1/α_1, α_2/α_3, α_4/β_3, α_5/β_4, and β_8/α_7 of AKeco*AP_5A, identified as flexible by SRLS. These are discussed below specifically.

The dynamic state of loops α_4/β_3 and α_5/β_4 can be related to the energetic counter-balancing of substrate binding concept set forth by Müller et al (*17*). On the basis of crystallographic B-factors, these authors found that in the AKeco-AP_5A complex the active site is rigid, whereas loops α_4/β_3 and α_5/β_4 are flexible. Conversely, in the ligand-free enzyme the active site is flexible, whereas loops α_4/β_3 and α_5/β_4 are rigid. The "solidification" of loops α_4/β_3 and α_5/β_4 upon substrate release is hypothesized to serve as a "counterweight" balancing the substrate binding energy. This hypothesis was confirmed by a previous ^{15}N NMR relaxation study (*26*). The present SRLS analysis indicates that loops α_4/β_3 and α_5/β_4 (except for residue 103) are rigid in AKeco, and representative residues of these loops are intrinsically flexible in AKeco*AP_5A. Residues R156 and D158 of loop β_8/α_7 are involved in binding to the AP_5A phosphates 3−5. They form one of the two salt bridges that were found to change the conformation of the hinge connecting LID and CORE in the crystal state (*21*). The flexibility of these residues in the transition state, of which AKeco*AP_5A is a mimic (*21*), may be related to the initiation of LID movement toward product release. Residue A11 of loop β_1/α_1 pertains to the P-loop. This residue participates in a dense mesh of hydrogen bonds that connects the inhibitor with the enzyme. Its flexibility may be related to the site where transition state dissociation commences. Finally, the chain segment of AKeco*AP_5A featuring the largest number of contiguous ns regime residues is loop α_2/α_3. In the ligand free enzyme, this chain segment is part of helix α_2 (*17*). Upon inhibitor binding, it becomes a turn-type structure with hydrogen bonds between residues $i + n$ and i, with $n = 3, 4, 5$ (*21*). Its flexibility, possibly of a loop-swinging type, may be related to the onset of AMPbd movement toward product release. This is similar to the role played by loop β_8/α_7 in the context of LID motion. Finally, it is of interest to point out that all of the AKeco*AP_5A loops featuring ns regime dynamics are located at the protein surface.

A comment on the ns regime residues of loops α_2/α_3 and α_5/β_4 of AKeco*AP_5A are in order. All of these residues feature relatively low NOEs (Figure 3c). Yet, originally some were fit with models 2 or 4. As pointed out previously, these are false mimima that can be identified and avoided by selecting appropriate starting points in the fitting process (*14*). Also, some of these residues were fit with model 5, which we found to feature parameters of lower accuracy (*62*).

CONCLUSIONS

Ligand-free adenylate kinase from *E. coli* is a relatively large particle diffusing with $\tau_m = 15.1$ ns correlation time. Domain CORE features a rigid structure with rapid small-amplitude N−H bond vector fluctuations. The catalysis-related AMPbd and LID domains are engaged in nanosecond domain motion and substantial microsecond to millisecond conformational exchange. The AP_5A-inhibitor bound form is outstandingly rigid and compact ($\tau_m = 11.6$ ns). The majority of its residues feature the conventional rigid rapidly fluctuating structure. The exceptions include loops β_1/α_1, α_2/α_3, α_4/β_3, α_5/β_4, and β_8/α_7, which feature nanosecond local motions. Loops α_4/β_3 and α_5/β_4 are associated with the "energetic counterweight balancing of substrate binding" hypothesis, which is borne out by the SRLS analysis. The other ns regime loops of AKeco*AP_5A may be related to the onset of domain motion toward product release. In general, SRLS ^{15}N relaxation is a powerful tool for elucidating intrinsic flexibility, notably, slow motions, in proteins. It is particularly promising in the context of multidomain enzymes, where domain motion is associated with catalysis.

ACKNOWLEDGMENT

E.M. gratefully acknowledges the hospitality of CSIT, FSU, Tallahassee, FL, during short visits promoting this work; we also thank CSIT for computational resources. We thank Dr. David Fushman (University of Maryland, College Park, MD) for sharing with us his program DYNAMICS.

SUPPORTING INFORMATION AVAILABLE

^{15}N T_1, T_2, and ^{15}N-{^1H} NOE data of *E. coli* adenylate kinase acquired at 14.1 and 18.79 T at 303 K (Table S1). ^{15}N T_1, T_2, and ^{15}N-{^1H} *NOE* data of *E. coli* adenylate kinase in complex with the inhibitor AP_5A acquired at 14.1 and 18.79 T at 303 K (Table S2). The results of SRLS fitting based on the combined AKeco data set, including estimated errors of the best-fit parameters (Table S3). The results of

SRLS fitting based on the combined AKeco*AP_5A data set, including estimated errors of the best-fit parameters (Table S4). The results of MF fitting based on the combined AKeco*AP_5A data set, including estimated errors of the best-fit parameters (Table S5).

REFERENCES

1. Kay, L. E. (1998) *Nat. Struct. Biol. 5*, 513−517.
2. Ishima, R., and Torchia, D. A. (2000) *Nat. Struct. Biol. 7*, 740−743.
3. Peng, J. W., and Wagner, G. (1994) in *Methods in Enzymology* (James, T. L., and Oppenheimer, N. J., Eds.) Vol. 239, pp 563−595, Academic Press, New York.
4. Lipari, G., and Szabo, A. (1982a) *J. Am. Chem. Soc. 104*, 4546−4559.
5. Lipari, G., and Szabo, A. (1982b) *J. Am. Chem. Soc. 104*, 4559−4570.
6. Clore, G. M., Szabo, A., Bax, A., Kay, L. E., Driscoll, P. C., and Gronenborn, A. M (1990) *J. Am. Chem. Soc. 112*, 4989−4991.
7. Tugarinov, V., Liang, Z., Shapiro, Yu. E., Freed, J. H., and Meirovitch, E. (2001) *J. Am. Chem. Soc. 123*, 3055−3063.
8. Polimeno, A., and Freed, J. H. (1993) *Adv. Chem. Phys. 83*, 89−210.
9. Polimeno, A., and Freed, J. H. (1995) *J. Phys. Chem. 99*, 10995−11006.
10. Liang, Z., and Freed, J. H. (1999) *J. Phys. Chem. B 103*, 6384−6396.
11. Barnes, J. P., Liang, Z., Mchaourab, H. S., Freed, J. H., and Hubbell, W. L. (1999) *Biophys. J. 76*, 3298−3306.
12. Liang, Z., Freed, J. H., Keyes, R., and Bobst, A. M. (2000) *J. Phys. Chem. B 104*, 5372−5381.
13. Lin, W. J., and Freed, J. H. (1979) *J. Phys. Chem. 83*, 379−401.
14. Tugarinov, V., Shapiro, Yu. E., Liang, Z., Freed, J. H., and Meirovitch, E. (2002), *J. Mol. Biol. 315*, 155−170.
15. Bennett, W. S., and Huber, R. (1984) *Crit. Rev. Biochem. 15*, 291−384.
16. Noda, L. (1973) Adenylate kinase in *The Enzymes* (Boyer, P. D., Ed.) Vol. 8, pp 279−305, Academic Press, New York.
17. Müller, C. W., Schlauderer, G. J., Reinstein, J., and Schulz, G. (1996) *Structure 4*, 147−156.
18. Gerstein, M., Lesk, A. M., and Chothia, C. (1994) *Biochemistry 33*, 6739−6749.
19. Vornhein, C., Schlauderer, G. J., and Schulz, G. (1995) *Structure 3*, 483−490.
20. Müller-Dickermann, H.-J., and Schulz, G. E. (1995) *J. Mol. Biol. 246*, 522−530.
21. Müller, C. W., and Schulz, G. (1992) *J. Mol. Biol. 224*, 159−177.
22. Berry, M. B., Meador, B., Bilderback, T., Liang, P., and Glaser, M. (1994) *Proteins: Struct. Funct. Genet. 19*, 183−198.
23. Sinev, M. A., Sineva, E. V., Ittah, V., and Haas, E. (1996) *Biochemistry 35*, 6425−6437.
24. Sinev, M. A., Sineva, E. V., Ittah, V., and Haas, E. (1996) *FEBS Lett. 397*, 273−276.
25. Richard, J. P., and Frey, P. A. (1978) *J. Am. Chem. Soc. 110*, 7757−7758.
26. Shapiro, Y. E., Sinev, M. A., Sineva, E. V., Tugarinov, V., and Meirovitch, E. (2000) *Biochemistry 39*, 6634−6664.
27. Freed, J. H. (1976) *Spin Labeling: Theory and Applications* (Berliner, L. J., Ed.) p 53, Academic Press, New York.
28. Freed, H. J., Nayeem, A., and Rananavare, S. B. (1994) *The Molecular Dynamics of Liquid Crystals* (Luckhurst, G. R., Veracini, C. A., Eds.) Chapter 12, pp 271−312, Kluwer Academic Publishers, The Netherlands.
29. Freed, J. H. (1977) *J. Chem. Phys. 66*, 4183−4199.
30. The analogies drawn between SRLS model 5 and reduced extended MF on one hand, and model 6 and extended MF on the other hand, are merely formal. For example, the $K = 1$ term of model 6 is associated with the local motion $K = 2$ term of extended MF (see below). Genuine SRLS/MF correspondence can be established in the mode-decoupled limit ($R^L \gg R^C$) based on a rigorous SRLS theory (*29*) validated in a perturbational approach for axial ordering (S^2_0 nonzero), and further extended to asymmetric ordering (S^2_0 and $S^2_2 = S^2_{-2}$ nonzero) (*13*). The spectral densities $j_K = j^1_K + j^2_K + j^3_K$ (to be called LF below) are given by eqs 10 and B6 of ref *13*. The term j^1_K represents free local diffusion ($(\tau_K)^{-1} = 6\,R^L_\perp + K^2(R^L_{||} - R^L_\perp)$, K = 0, 1, 2), whereas the sum $j^2_K + j^3_K$ represents the SRLS contributions. If the local ordering tensor is assumed to be axially symmetric and the diffusion tilt angle β_{MD} is zero, only $j_{K=0}$ contributes to $J(\omega)$(LF). In this case, $J(\omega)$(LF) corresponds formally to the original MF formula (*4*, *5*) with $(S^2_0)^2$ corresponding to the squared generalized MF order parameter and τ_0 to the effective MF local motion correlation time, τ. For anisotropic local motion all of the components of j_K contribute to $J(\omega)$(LF). If β_{MD} is set equal to 90°, the $K = 1$ contribution of j^1_K vanishes (the coefficient B in eq 5 of this paper is zero). In this case, $J(\omega)$(LF) corresponds formally to the extended MF formula (*6*) with $\tau_0 = \tau_s$, $\tau_2 = \tau_f$, and $(S^2_0)^2$ and $(S^2)^2$ recast in terms of S_f^2 and S_s^2. If in addition $\tau_2 \ll \tau_0$, the reduced extended MF formula is obtained. We now consider the applicability of the MF formulas to N−H bond motion. The extended MF formula was introduced particularly to allow for a small time scale separation between τ_s and τ_m. This obliterates one of the two basic conditions underlying the perturbation approach, invalidating the applicability of this spectral density to N−H bond dynamics. In this parameter range mode-coupling dominates the spectral density and the complete SRLS theory must be used. With the original MF formula large time scale separation between τ and τ_m is implicit, but the condition that S^2 be small is not fulfilled. In this limit the dominant effect is reduction of τ through renormalization by the high local potentials (*31*, *32*). Although in SRLS mode-coupling effects are also involved, they were found to be small, to the extent that the functional form of the original MF formula is largely preserved and may be used. However, τ calculated by MF should be considered as an effective value reduced several-fold by potential-induced renormalization.
31. Polnaszek, C. F., Bruno, G. V., and Freed, J. H. (1973) *J. Chem. Phys. 58*, 3185−3199.
32. Polnaszek, C. F., and Freed, J. H. (1975) *J. Phys. Chem. 79*, 2283−2306.
33. Fushman, D., and Cowburn, D. (1999) *J. Biomol. NMR 13*, 139−147.
34. Abragam, A. (1961) *Principles of Nuclear Magnetism*, Oxford University Press (Clarendon), London.
35. Reinstein, J., Brunne, M., and Wittinghofer, A. (1988) *Biochemistry 27*, 4712−4720.
36. Girons, I. S., Gilles, A.-M., Margarita, D., Michelson, S., Monnot, M., Fermandjian, S., Danchin, A., and Barzu, O. (1987) *J. Biol. Chem. 262*, 622−629.
37. Delaglio, F., Grzesiek, S., Vuister, G. W., Zhu, G., Pfeifer, J., and Bax, A. (1995) *J. Biomol. NMR 6*, 277−293.
38. Burlacu-Miron, S., Perrier, V., Gilles, A.-M., Mispelter, J., Barzu, O., and Craescu, C. T. (1999) *J. Biomol. NMR 13*, 93−94.
39. Meirovitch, E., Sinev, M. A., and Sineva, E. V. (1999) *J. Biomol. NMR 13*, 195−196.
40. Vold, R. L., Waugh, J. S., Klein, M. P., and Phelps, D. E. (1968) *J. Chem. Phys. 48*, 3831−3832.
41. Meiboom, S., and Gill, D. (1958) *Rev. Sci. Instrum. 29*, 688−691.
42. Noggle, J. H., and Shirmer, R. E. (1971) *The Nuclear Overhauser Effect: Chemical Aplication*, Academic Press, New York.
43. Kay, L. E., Nicholson, L. K., Delaglio, F., Bax, A., and Torchia, D. A. (1992) *J. Magn. Res. 97*, 359−375.
44. Palmer, A. G., III., Skelton, N. J., Chazin, W. J., Wright, P. E., and Rance, M. (1992) *Mol. Phys. 75*, 699−711.
45. Grzesiek, S., and Bax, A. (1993) *J. Am. Chem. Soc. 115*, 12593−12594.
46. Live, D. H., Davis, D. G., Agosta, W. C., and Cowburn, D. (1984) *J. Am. Chem. Soc. 106*, 1939−1941.

47. Palmer, A. G., III., Rance, M., and Wright, P. E. (1991) *J. Am. Chem. Soc. 113*, 4371−4380.
48. Fushman, D., Tjandra, N., and Cowburn, D. (1998) *J. Am. Chem. Soc. 120*, 10947−10952.
49. Press, W. H., Teukolsky, S. A., Vetterling, W. T., and Flannery, B. P. (1992) *Numerical Recipes in C. The Art of Scientific Computing*, Cambridge University Press.
50. Kamath, U., and Shriver, J. W. (1989) *J. Biol. Chem. 264*, 5586−5592.
51. Mandel, A. M., Akke, M., and Palmer, A. G., III. (1995) *J. Mol. Biol. 246*, 144−163.
52. Burlacu-Miron, S., Gilles, A. M., Popescu, A., Barzu, O., and Craescu, C. T. (1999) *Eur. J. Biochem. 264*, 765−774.
53. Brüschweiler, R., Liao, X., and Wright, P. E. (1995) *Science 268*, 886−889.
54. Lee, L. K., Rance, M., Chazin, W. J., and Palmer, A. G., III. (1997) *J. Biomol. NMR 9*, 287−298.
55. Millet, O., Loria, J. P., Kroenke, C. D., Pons, M., and Palmer, A. G., III. (2000) *J. Am. Chem. Soc. 122*, 2867−2877.
56. Fushman, D., and Cowburn, D. (1998) *J. Am. Chem. Soc. 120*, 7109−7110.
57. Fushman, D., Cahill, S., and Cowburn, D. (1997) *J. Mol. Biol. 266*, 173−194.
58. Kay, L. E., Torchia, D. A., and Bax, A. (1989) *Biochemistry 28*, 8972−8979.
59. Tjandra, N., Szabo, A., and Bax, A. (1996) *J. Am. Chem. Soc. 118*, 6986−6991.
60. Lienin, S. F, Bremi, T., Brutcher, B., Brüschweiler, R., and Ernst, R. R. (1998) *J. Am. Chem. Soc. 129*, 9870−9879.
61. Schulz, G. E., and Schirmer, R. H. (1990) *Principles of Protein Structure* (Cantor, C. R., Ed.) Springer-Verlag, New York.
62. The VALM spectral density is given by $J(\omega) = Aj_{K=0}$, with $j_{K=0}$ calculated for a local diffusion tensor component $R^{L}{}_{\perp}$. This approximation has been validated by extrapolation for $\tau_{||}/\tau_{\perp} \rightarrow 0$, when $j_{K=1}$ and $j_{K=2}$ become negligibly small as compared to $j_{K=0}$, with $Aj_{K=0} \gg Bj_{K=1}$, $Cj_{K=2}$ in eq 5 ($\beta_{MD} \approx 20°$, yielding $A = 0.68$, $B = 0.31$, and $C = 0.09$). In this study, $\tau_{||}/\tau_{\perp} = (4.5-8.0) \times 10^{-4}$. Despite the apparently low value of this ratio, $j_{K=1}$ was found to be large enough to render the contribution of $Bj_{K=1}$ to $J(\omega)$ on the order of 20% (the contribution of $Cj_{K=2}$ is negligible). The slow convergence of $j_{K=1}$ and $j_{K=2}$ to zero as $\tau_{||}/\tau_{\perp} \rightarrow 0$ is a characteristic of the $R^{L}{}_{\perp} \approx R^{C}$ parameters range, where mode-coupling between $R^{L}{}_{\perp}$ and R^{C} is very effective. This is why SRLS fitting based on two-field data selects in the ns regime predominantly models 6 and 8, rather than 5 and 7. When model 5 is occasionally selected on statistical grounds, the pertinent parameters are of lower accuracy, having absorbed the omitted contribution of the mixed $R^{L}{}_{\perp}$ and R^{C} modes to $j_{K=1}$.
63. Kraulis, P. J. (1991) *J. Applied Crystall. 24*, 946−995.

BI012132Q